## **OPEN ACCESS**



# The Cold and Dusty Circumstellar Matter around Fast-expanding Type Ia Supernovae

Xiaofeng Wang <sup>1</sup> D, Jia Chen <sup>1</sup>, Lifan Wang <sup>2,3</sup>, Maokai Hu <sup>3</sup>, Gaobo Xi <sup>1</sup>, Yi Yang <sup>2,4</sup>, Xulin Zhao <sup>1,5</sup>, and Wenxiong Li <sup>1</sup> Physics Department and Tsinghua Center for Astrophysics, Tsinghua University, Beijing 100084, People's Republic of China; wang\_xf@mail.tsinghua.edu.cn <sup>2</sup> Mitchell Institute for Fundamental Physics and Astronomy, Texas A&M University, College Station, TX 77843, USA <sup>3</sup> Purple Mountain Observatory, Nanjing, 201008, Jiangsu, People's Republic of China

Department of Particle Physics and Astrophysics, Weizmann Institute of Science, Rehovot 76100, Israel
 Department of Physics, Tianjin University of Technology, Tianjin 300384, People's Republic of China Received 2018 October 28; revised 2019 May 27; accepted 2019 May 30; published 2019 September 9

#### Abstract

SNe Ia play key roles in revealing the accelerating expansion of the universe, but our knowledge of their progenitors is still very limited. Here we report the discovery of a rigid dichotomy in circumstellar (CS) environments around two subclasses of SNe Ia as defined by their distinct photospheric velocities. For the SNe Ia with high photospheric velocities (HVs), we found a significant excess flux in blue light 60–100 days past maximum, while this phenomenon is absent for SNe with normal photospheric velocity. This blue excess can be attributed to light echoes by circumstellar dust located at a distance of about  $(1-2) \times 10^{17}$  cm from the HV subclass. Moreover, we also found that the HV SNe Ia show systematically evolving Na I absorption line by performing a systematic search of variable Na I absorption can be modeled in terms of photoionization model, with the location of the gas clouds at a distance of about  $2 \times 10^{17}$  cm, in striking agreement with the location of CS dust inferred from *B*-band light-curve excess. These observations show clearly that the progenitors of HV subclass are likely from single-degenerate progenitor system (i.e., symbiotic binary), while the NV subclass may arise from double-degenerate system.

Key words: binaries: symbiotic - scattering - stars: circumstellar matter - supernovae: general

Supporting material: machine-readable table

#### 1. Introduction

It is conventionally accepted that SNe Ia result from thermonuclear explosion of a carbon-oxygen (CO) white dwarf (Nomoto et al. 1997; Hillebrandt & Niemeyer 2000; Maoz et al. 2014). Two popular scenarios are: merger-induced explosion of two white dwarfs (the so-called double-degenerate (DD) scenario) and accretion-induced explosion of a massive WD with a non-degenerate companion (the so-called singledegenerate (SD) scenario). Many progenitor classes have been proposed (Gilfanov & Bogdán 2010; Wang & Han 2012; Maoz et al. 2014), but observational evidence has not yet reached definitive conclusions on particular progenitor systems. The SD scenario is favored by the possible detections of circumstellar material (CSM) around some SNe Ia through detections of strong ejecta-CSM interaction (Hamuy et al. 2003; Wang et al. 2004; Aldering et al. 2006; Taddia et al. 2012; Silverman et al. 2013; Bochenek et al. 2018) or evolving narrow absorption lines possibly due to CSM (Patat et al. 2007; Blondin et al. 2009; Sternberg et al. 2011; Dilday et al. 2012), while there are also observational findings suggesting no companion signatures for some SNe Ia (Li et al. 2011a; González-Hernández et al. 2012; Schaefer & Pagnotta 2012; Olling et al. 2015). This may suggest that SNe Ia have multiple progenitor systems, as favored by the discovery that SNe Ia with different ejecta velocities originate from distinct birthplace environments (Wang et al. 2013).

Original content from this work may be used under the terms of the Creative Commons Attribution 3.0 licence. Any further distribution of this work must maintain attribution to the author(s) and the title of the work, journal citation and DOI.

Observationally, spectroscopically normal SNe Ia consist of  $\sim$ 70% of all SNe Ia (Branch et al. 1993; Li et al. 2011b) and can be categorized into high-velocity (HV) and normal-velocity (NV) subclasses based on ejecta velocities inferred from the blueshifted Si II 6355 Å line, i.e., 12,000 km s<sup>-1</sup> (Wang et al. 2009a). Compared to NV ones, HV SNe Ia have systematically redder B-V colors at maximum light and prefer abnormally low total to selective absorption  $R_V$  ratios (Wang et al. 2009a). It is thus important to examine whether this difference arises from the intrinsic difference of the SN ejecta or from systematic difference in circumstellar (CS) and/or interstellar environments of the two groups. These issues may shed light on the elusive progenitor systems of SNe Ia.

The presence of CS dust can be tested by examining the behaviors of narrow interstellar absorption features. The interstellar sodium Na I doublet (D<sub>1</sub> 5896 Å, D<sub>2</sub> 5890 Å) is a good tracer of gas, dust, and metals, and its strength is found to show positive correlation with line-of-sight dust reddening (Munari & Zwitter 1997; Turrato et al. 2003; Blondin et al. 2009; Folatelli et al. 2010; Pozanski et al. 2012; Phillips et al. 2013). Its evolution (or variation) and velocity structure can provide significant constraints on the presence and distance of CS dust around SNe Ia (Patat et al. 2007; Chugai 2008; Simon et al. 2009; Sternberg et al. 2011), while it is not clear why evolution or velocity structure of interstellar Na I lines exist in some SNe Ia but not in the others. On the other hand, the surrounding CS dust may also affect the light curves of SNe Ia as a result of light scattering by the nearby dust. This can be examined by inspecting light curves in the early nebular phase.

In this paper, we conducted a systematic search for variable Na I absorption in low-resolution spectra of SNe Ia as well as an overall analysis of the behavior of their late-time light curves, in an attempt to constrain the dust environments around SNe Ia and hence the properties of their progenitors. This paper is organized as follows. In Section 2, we describe the data set of SNe Ia used in our analysis. The results from interstellar Na absorptions and late-time light curves are presented in Section 3. Discussions and conclusions are given in Section 4.

#### 2. Data set

The spectral samples used to measure the Na absorption features in SNe Ia are primarily from the Center for Astrophysics (CfA) Supernova Program (Riess et al. 1999), and the Carnegie Supernova Project (CSP; Hamuy et al. 1996). The former sample contains 2603 spectra of 462 nearby SNe Ia (Blondin et al. 2012), and most (94%) of which were obtained with the FAST spectrograph on the 1.5 m telescope at the Fred Lawrence Whipple Observatory (FLWO). The latter data set contains 604 spectra of 93 SNe Ia (Folatelli et al. 2013), which were mainly obtained with the 2.5 m du Pont Telescope at Las Campanas Observatory. All of the spectra were reduced in a consistent way and have a typical FWHM resolution of 6–7 A, providing the largest homogeneous spectroscopic data set of SNe Ia. We also used the spectra from the Berkeley Supernova Program (BSP, Silverman & Filippenko 2012), consisting of 1298 spectra for 582 SNe Ia, to get further classifications of our SN Ia sample and measure the Na absorptions whenever necessary. The spectral phases were obtained with respect to the B-band maximum light, based on the published light curves of CfA (Riess et al. 1999; Jha et al. 2006; Hicken et al. 2009, 2012), the Lick Observatory Supernova Survey (LOSS, Ganeshalingam et al. 2010), and the Carnegie Supernova Project (Contreras et al. 2010; Stritzinger et al. 2011; Krisciunas et al. 2017). The light-curve parameters, including the peak magnitudes, the  $B_{\rm max}-V_{\rm max}$  colors at the maximum light, and the post-maximum decline rates  $\Delta m_{15}(B)$  (Phillips 1993) are estimated by applying polynomial fits and/or the SALT2 fit (Guy et al. 2007) to the observed data. A weighted average is adopted when the estimations from the above two methods are both reasonable. The measurement results and relevant photometric parameters for each SN sample are listed in Table 1.

To eliminate the effects from noise spikes on the continuum determination of Na I absorption doublet, we smoothed the observed spectra in the range of  $5850 \sim 5950\,\text{Å}$  (after corrections for the redshift of host galaxies) using a Gaussian function with an FWHM ( $\sim 2.35\sigma$ ) of 7 Å. This amount is chosen because it is comparable to the typical width of the Na I absorption doublet in the spectra used in our analysis and this match can also optimize the resolution of signal from noise according to the matched filter theorem. The smoothed spectra are then used to find the local flux maximum and hence define the pseudo-continuum. The definition of pseudo-continuum and hence the calculations of the EW are automatic for our SN sample, but we also double-checked the integration limits by eyes to make sure that they are reasonably determined. For a few SNe whose spectra suffering from improper wavelength calibration and/or motion of the SNe relative to the galaxy center (e.g., SN 1998eg and SN 2007ai), we adjusted their integration limit manually. As the Na I D absorption of some SNe Ia is found to show temporal evolution within one week from the maximum light (see also Figure 2), the EW of each

SN is taken as a weighted mean of the results obtained at  $t \sim 0$ -30 days after the maximum light when multi-epoch spectra are available.

As late-time photometric evolution can provide an important probe of dust environments around SNe Ia, we thus also include sample with better photometric observations in the early nebular phase even though they may not have good spectral data allowing for accurate measurement of Na I D absorption. The total sample thus contains 206 SNe Ia, including subtypes of 112 NV, 54 HV, 25 91T-like, and 15 91bg-like objects, which corresponds to a percentage of 54.4%, 26.2%, 12.1%, and 7.3%, respectively. These fractions of different subtypes are basically consistent with the ones obtained with a magnitude-limited sample of SNe Ia (i.e., Li et al. 2011b).

Table 1 lists the relevant parameters of our SN Ia sample. The meaning of each column is as follows: column (1) SN name; column (2) the SN Ia subtype based on the Si II velocity at around the maximum light (Wang et al. 2009a); column (3) ejecta velocity measured from Si II 6355 absorption in the near-maximum-light spectra, estimated using the multiple-Gaussian technique described in Zhao et al. (2015); column (4)  $\Delta m_{15}(B)$ , the *B*-band magnitude decline rate in 15 days from the maximum; column (5),  $B_{\rm max} - V_{\rm max}$  color at the maximum light, corrected for the Galactic reddening; column (6) the weighted mean value of the equivalent width (EW) of Na I absorption over the period  $0 \lesssim t \lesssim 30$  days whenever possible; column (7) the *B*-band magnitude decline in the first 60 days after the *B*-band maximum; column (8) the *V*-band magnitude decline in the first 60 days after the *V*-band maximum; column (9) references.

#### 3. Results

## 3.1. Narrow Na I Absorption Features

Figure 1 shows the B-V colors at the maximum light versus the EWs of the NaID absorption due to the host galaxies. Foreground Galactic reddening corrections have been removed from the observed colors. The  $B_{\rm max}-V_{\rm max}$  color has usually been used as an indicator of reddening (Phillips et al. 1999; Wang et al. 2009b; Folatelli et al. 2010, and Burns et al. 2014), though the subclasses of 91T-like and 91bg-like SNe Ia tend to have peculiar colors and they are thus not shown in Figure 1.

As can be readily seen, the correlation between the  $B_{\rm max}-V_{\rm max}$  color and the strength of Na absorption is apparent for the HV and NV subclasses, with stronger Na I D absorptions corresponding to redder colors (and hence larger reddening). However, these two subclasses of SNe Ia show noticeable differences in the distribution of their  $B_{
m max}-V_{
m max}$ colors and the Na I D EWs. A two-dimensional Kolmogoroff-Smirnoff (KS) test gives a probability of 0.01% that they have statistically identical Na I D EW and color distribution. Examining the EW of Na I absorption and the  $B_{\rm max}-V_{\rm max}$ color separately yields a respective probability of 1.4% and 0.0002% that the two subclasses have the same parent distribution. The mean  $B_{\rm max}-V_{\rm max}$  colors estimated for these two subclasses are 0.26 mag (HV) and 0.08 mag (NV), respectively, while the mean Na I D EWs are 1.1 Å (HV) and 0.7 Å (NV), respectively. In general, the HV subclass have redder colors and stronger Na I D absorption lines, and the fraction found with EWs  $\gtrsim 1.0$  is as high as 44.8% (versus

 Table 1

 Summary of Classification, Spectroscopic, and Photometric Properties of the SN Ia Sample

SN Name	SN Type	$(\times 10^{4}  \mathrm{km \ s^{-1}})$	$\Delta m_{15}(B)$ (mag)	$B_{ m max} - V_{ m max} \ ({ m mag})$	EW (Å)	$\Delta m_{60}(B)$ (mag)	$\Delta m_{60}(V)$ (mag)	References
				Branch normal				
SN 1984A	HV	1.47(04)	1.22(10)	0.16(09)		3.10(10)	2.59(05)	1
SN 1989B	NV	1.05(03)	1.35(05)	0.32(09)	3.17(19)	3.41(06)	•••	2
SN 1994M	HV	1.24(02)	1.47(06)	0.10(04)	0.22(21)	•••	•••	3, 4, 5
SN 1994ae	NV	1.11(03)	0.89(05)	-0.05(04)	0.29(06)	3.46(03)	2.60(03)	3, 4, 6
SN 1995D	NV	1.01(02)	1.01(03)	0.01(03)	0.33(09)	3.32(03)	2.47(03)	3, 4, 5
SN 1995E	NV	1.08(02)	1.20(07)	0.69(05)	1.97(39)	•••	2.49(05)	3, 4, 5
SN 1995al	HV	1.25(03)	0.95(05)	0.09(04)	1.04(06)	3.25(05)	2.48(06)	4, 5
SN 1996C	NV	1.08(03)	0.95(03)	0.09(04)	•••	3.23(05)	2.58(04)	4, 5
SN 1996X	NV	1.13(03)	1.30(05)	-0.01(03)	0.00(12)	3.55(05)	2.72(04)	3, 4, 5
SN 1996Z	NV	1.17(03)	1.18(18)	0.26(07)	1.51(17)	•••	•••	4, 5
SN 1996ai	NV	1.06(02)	1.00(08)	1.47(07)	>2.8	•••	•••	3, 4, 5
SN 1996bo	HV	1.23(05)	1.31(06)	0.36(04)	1.63(16)			4, 5
SN 1997E	NV	1.18(03)	1.42(05)	0.05(03)	0.10(20)	3.60(03)	2.83(05)	4, 7
SN 1997Y	NV	1.11(03)	1.39(05)	0.01(03)	1.23(21)			4, 7
SN 1997bp	HV	1.57(05)	1.11(03)	0.21(03)	1.85(09)	3.13(05)	2.48(03)	4, 7
SN 1997bq	HV	1.45(05)	1.13(10)	0.10(04)	0.51(07)	•••	•••	4, 7
SN 1997do	HV	1.25(05)	1.08(03)	0.13(04)	0.17(26)	3.30(07)	2.46(05)	7, 8
SN 1998V	NV	1.09(03)	0.98(04)	0.03(03)	0.26(10)	•••	•••	3, 7, 8
SN 1998aq	NV	1.07(02)	1.02(03)	-0.08(03)	0.16(08)	3.51(02)	2.62(02)	6, 8
SN 1998bu	NV	1.08(03)	1.06(04)	0.33(03)	0.45(10)	3.34(03)	2.60(04)	8, 9
SN 1998dh	NV	1.18(02)	1.22(04)	0.07(03)	0.36(12)	3.33(03)	2.64(03)	8, 10
SN 1998dk	HV	1.26(03)	1.15(03)	0.17(06)	1.15(17)	•••	•••	3, 4
SN 1998dm	NV	1.02(03)	0.96(05)	0.27(05)	0.62(13)	3.34(03)	2.55(03)	8, 10
SN 1998ec	HV	1.26(03)	1.18(04)	0.22(07)	1.07(23)	•••	•••	8, 10
SN 1998ef	HV	1.24(05)	1.36(06)	-0.04(04)	0.31(12)	3.40(04)	2.62(03)	4, 10
SN 1998eg	NV	1.05(03)	1.21(06)	0.02(03)	1.49(18)	•••	•••	6, 8, 10
SN 1999cl	HV	1.22(03)	1.26(05)	1.08(04)	3.45(08)	•••	•••	4, 8, 10
SN 1999cp	NV	1.09(03)	1.01(03)	0.02(03)	0(08)	•••	•••	3, 4, 10
SN 1999dk	HV	1.26(06)	1.15(05)	0.08(03)	0.10(10)	3.30(04)	2.65(04)	3, 10
SN 1999ej	NV	1.07(03)	1.57(08)	0.04(03)	0(11)	3.53(06)	2.80(06)	8, 10
SN 2000cn	NV	1.15(05)	1.68(06)	0.12(03)	0(15)	3.46(10)	2.84(06)	8, 10
SN 2000cp	NV	1.15(03)	1.24(04)	0.41(04)	2.64(19)	•••	•••	3, 4, 10
SN 2000cw	NV	1.06(03)	1.33(05)	0.06(03)	0(14)	•••	•••	3, 4, 7
SN 2000dk	NV	1.09(03)	1.66(03)	0(03)	0.10(14)	3.64(07)	3.00(03)	3, 8, 10
SN 2000dm	NV	1.12(03)	1.51(04)	0.02(03)	0(06)		•••	3, 4, 10
SN 2000dn	NV	1.03(03)	1.13(03)	-0.03(03)	0(20)	•••	•••	3, 4, 10
SN 2000dr	NV	1.05(05)	1.73(10)	0.11(04)	•••	3.73(13)	3.07(10)	3, 10
SN 2000fa	NV	1.18(03)	0.98(09)	0.11(03)	0.97(19)	3.29(04)	2.58(03)	3, 8, 7, 10
SN 2001E	HV	1.40(05)	1.08(05)	0.43(04)	1.44(24)			4, 10
SN 2001ay	HV	1.44(02)	0.68(05)	0.06(06)	0.71(15)	•••	•••	4, 10
SN 2001bf	NV	1.10(03)	0.83(03)	0.03(03)	0(12)	3.00(07)	2.23(04)	3, 4, 10
SN 2001bg	HV	1.23(03)	1.14(03)	0.15(03)	1.02(09)	•••	•••	4, 10
SN 2001br	HV	1.35(03)	1.32(06)	0.10(03)	1.10(21)	•••	•••	4, 10
SN 2001ck	NV	1.15(04)	1.09(04)	-0.01(03)	1.24(20)	•••	•••	4, 10
SN 2001cp	NV	1.07(03)	0.90(04)	0.04(03)	0.63(18)	•••	•••	4, 10
SN 2001 da	NV	1.17(03)	1.30(04)	0.17(03)	0.71(12)	3.26(06)	2.54(03)	4, 10
SN 2001en	HV	1.30(03)	1.23(03)	0.04(02)	0.98(14)	3.35(05)	2.69(04)	4, 10
SN 2001ep	NV	1.05(03)	1.40(05)	0.08(02)	0.73(20)	3.55(05)	2.69(05)	4, 10
SN 2001fe	NV	1.09(02)	0.96(10)	-0.03(03)	0.71(16)	3.39(05)	2.57(03)	3, 11
SN 2002aw	NV	1.06(02)	1.15(03)	0.08(03)	1.06(21)	3.50(07)	2.51(04)	3, 4, 10
SN 2002bf	HV	1.61(04)	1.08(10)	0.17(05)	1.18(24)	3.14(05)	2.57(04)	4, 10
SN 2002bo	HV	1.32(02)	1.15(03)	0.40(08)	2.44(09)	3.18(03)	2.56(02)	4, 10
SN 2002cd	HV	1.50(03)	0.94(06)	0.63(04)	1.71(10)	2.96(10)	2.51(04)	3, 4, 10, 11
SN 2002cr	NV	0.98(02)	1.19(05)	0(02)	0.51(12)	3.45(04)	2.60(03)	4, 10
SN 2002cs	HV	1.36(06)	1.07(05)	0.12(03)	•••	3.18(04)	2.10(03)	4, 10
SN 2002cu	HV	1.23(05)	1.48(04)	0.07(03)	0(20)	3.48(06)	2.84(04)	3, 4, 10
SN 2002de	NV	1.13(02)	1.05(03)	0.16(03)	1.60(32)	3.40(08)	2.70(06)	4, 10
SN 2002dj	HV	1.34(02)	1.13(03)	0.07(03)	0.80(13)	3.29(10)	2.57(08)	4, 10
SN 2002dp	NV	1.07(02)	1.28(03)	0.07(02)	0.70(14)	3.45(04)	2.62(03)	4, 10
SN 2002eb	NV	1.03(02)	0.93(03)	-0.03(03)	0(20)	3.34(04)	2.44(06)	3, 10
SN 2002ef	HV	1.16(04)	1.18(05)	0.32(04)	1.99(32)	3.36(09)	2.64(04)	3, 4, 10
				0.12(03)	1.75(09)		2.65(04)	10, 12

Table 1 (Continued)

SN Name	SN Type	$(\times 10^{4}  \mathrm{km \ s^{-1}})$	$\Delta m_{15}(B)$ (mag)	$B_{ m max} - V_{ m max} \ ({ m mag})$	EW (Å)	$\Delta m_{60}(B)$ (mag)	$\Delta m_{60}(V)$ (mag)	References
SN 2002fk	NV	0.98(03)	1.02(03)	-0.10(03)	0.07(08)	3.43(03)	2.61(03)	4, 10
SN 2002 ha	NV	1.09(03)	1.37(03)	-0.02(03)	0.83(16)	•••	2.82(29)	3, 4, 10
SN 2002he	NV	1.16(05)	1.41(05)	0.02(03)	0(10)	3.53(07)	2.78(10)	3, 4, 10
SN 2002hu	NV	1.04(03)	1.02(03)	-0.07(03)	•••	•••	2.45(21)	3, 4, 11
SN 2002jg	NV	1.09(03)	1.49(07)	0.67(06)	2.70(50)	•••	•••	4, 10
SN 2003W	HV	1.51(04)	1.15(03)	0.16(04)	0.99(20)	3.05(09)	2.54(06)	4, 10, 11
SN 2003cg	NV	1.09(03)	1.17(04)	1.14(04)	5.43(23)	3.39(03)	2.62(03)	4, 10, 11
SN 2003du	NV	1.04(03)	1.00(02)	-0.06(03)	0.10(07)	3.38(03)	2.60(03)	4, 10, 11, 13
SN 2003gn	HV	1.23(03)	1.30(08)	0.10(03)	•••	3.59(10)	2.90(10)	3, 4, 10
SN 2003hv	NV	1.13(03)	1.45(07)	-0.08(04)	0(10)	3.59(04)	2.92(03)	3, 4, 10
SN 2003kf	NV	1.11(03)	0.93(04)	0.02(03)	0.50(10)	3.37(10)	2.57(03)	3, 4, 10, 11
SN 2004L	NV	1.02(02)	1.42(10)	0.23(05)	1.15(23)			3, 4, 11
SN 2004S	NV	0.97(03)	1.08(07)	-0.04(05)	0(20)	3.45(05)	2.61(04)	10, 14
SN 2004as	HV	1.21(03)	1.20(05)	0.09(03)	0.26(25)	3.41(05)	2.59(03)	3, 4, 10, 11
SN 2004at	NV	1.09(02)	1.07(03)	-0.06(03)	0.19(14)	3.46(06)	2.64(03)	4, 10
SN 2004bg	NV	1.04(03)	1.12(07)	-0.08(03)	0(20)	3.54(03)	2.76(06)	4, 10
SN 2004bk	HV	1.22(05)	0.98(08)	0.06(04)	0.47(12)	3.34(06)	2.63(06)	3, 4, 10
SN 2004dt	HV	1.39(03)	1.10(05)	-0.01(03)	0.46(21)	3.15(05)	2.51(05)	10, 15
SN 2004ef	HV	1.20(05)	1.42(03)	0.09(03)	0.90(27)	3.36(04)	2.75(04)	4, 16
SN 2004eo	NV	1.07(03)	1.40(03)	0.03(03)	0(20)	3.48(04)	2.69(04)	16, 17
SN 2004ey	NV	1.11(03)	1.03(03)	-0.10(03)	0(30)	3.44(04)	2.47(05)	3, 10, 16, 18
SN 2004fz	NV	1.02(03)	1.34(04)	0.01(03)	0.30(20)			4, 10
SN 2004gs	NV	1.08(03)	1.50(05)	0.15(02)	1.47(15)	3.56(04)	2.95(03)	4, 16, 18
SN 2004gu	NV	1.10(03)	0.82(03)	0.12(03)	1.63(16)	•••	•••	16, 18
SN 2005A	HV	1.42(03)	1.19(05)	1.00(03)	3.50(20)	•••	•••	16, 18
SN 2005W	NV	1.08(02)	1.19(03)	0.14(03)	0.76(15)			16, 18
SN 2005ag	NV	1.13(03)	1.04(05)	-0.02(03)		3.19(04)	2.64(03)	16, 18
SN 2005al	NV	1.09(03)	1.23(05)	-0.07(03)	0(10)	3.53(03)	2.82(05)	16, 18
SN 2005am	NV	1.18(02)	1.45(06)	0.04(03)	0.21(10)	3.50(05)	2.87(05)	4, 10, 16
SN 2005bc	NV	1.08(03)	1.45(06)	0.43(05)	1.90(25)	3.53(06)	2.86(07)	3, 4, 10
SN 2005bg SN 2005bo	NV	1.07(02)	0.99(05)	0(03) 0.26(04)	1.07(11)	2.59(10)	2.70(06)	16, 18
SN 200566	NV NV	1.09(02)	1.30(05)	0.26(04)	1.38(14)	3.58(10)		4, 10, 16, 18 19
SN 2005de	NV NV	1.01(03) 1.03(03)	1.07(03) 1.19(05)	0.01(03)	0.30(06) 0.51(10)	3.42(03) 3.47(07)	2.54(04) 2.62(04)	3, 10
SN 2005de SN 2005el	NV	1.05(03)	1.30(03)	-0.09(03)	0.20(18)	3.46(05)	2.80(06)	3, 4, 10, 16
SN 2005er	NV	1.13(03)	0.96(05)	-0.09(03) -0.01(03)	0.20(18)	3.40(03)	2.64(05)	4, 16, 18
SN 2005iq	NV	1.10(05)	1.30(03)	-0.01(03) -0.09(03)	0(24)	3.62(06)	2.87(06)	3, 4, 16
SN 2005kc	NV	1.04(02)	1.16(10)	0.25(04)	1.78(13)	5.02(00)	2.87(00)	3, 16, 18
SN 2005ki	NV	1.10(02)	1.43(06)	-0.09(03)	0.30(09)	3.54(04)	2.87(03)	3, 16, 18
SN 2005lu	HV	1.37(10)	0.97(03)	0.19(03)	2.02(32)	3.21(05)	2.56(04)	16, 18
SN 2005ms	NV	1.13(03)	1.02(07)	-0.03(03)	0(20)	3.38(05)	2.67(11)	3, 11
SN 2005na	NV	1.04(02)	1.08(07)	-0.08(03)	0(23)	3.48(03)	2.62(02)	3, 4, 16
SN 2006D	NV	1.08(02)	1.33(06)	0.03(03)	0(05)	3.50(03)	2.91(02)	3, 4, 16, 18
SN 2006N	NV	1.14(02)	1.52(08)	0.01(03)	0.82(21)	3.94(10)	2.97(05)	3, 4, 11
SN 2006S	NV	1.10(02)	0.91(04)	0.04(03)	0.46(09)		2.50(10)	3, 4, 11
SN 2006X	HV	1.61(02)	1.26(05)	1.23(04)	2.05(08)	2.97(03)	2.48(02)	11, 16, 20
SN 2006ac	HV	1.32(06)	1.23(08)	0.04(03)	0(13)	3.40(08)	2.72(05)	4, 11
SN 2006ax	NV	1.01(02)	1.00(04)	-0.08(02)	0(12)	3.43(05)	2.55(04)	3, 4, 11, 16
SN 2006cp	HV	1.27(06)	1.09(05)	0.06(03)	0.26(14)			3, 4, 10, 11
SN 2006ef	HV	1.23(03)	1.37(06)	-0.01(03)	0.50(10)	3.52(05)	2.86(05)	3, 10
SN 2006ej	HV	1.22(05)	1.38(07)	0(05)	0(23)	3.41(05)	2.82(05)	3, 10, 21
SN 2006en	NV	1.06(03)	1.12(05)	0.10(03)	1.22(24)			3, 10
SN 2006et	NV	0.97(03)	0.93(03)	0.16(02)	5.19(23)	3.35(04)	2.55(03)	3, 4, 21
SN 2006gr	HV	1.34(07)	0.91(05)	0.11(03)	1.48(23)		2.61(08)	4, 10, 11
SN 2006hb	NV	1.00(03)	1.55(09)	0.04(03)	0.10(21)	3.63(04)	2.93(04)	4, 18, 21
SN 2006is	HV	1.38(05)	0.63(04)	-0.05(03)	0.23(20)	3.02(04)	2.45(03)	18, 21
SN 2006le	NV	1.18(06)	0.89(05)	-0.03(03)	0.10(08)	3.26(07)	2.56(04)	4, 10, 11
SN 2006os	NV	1.16(03)	1.23(07)	0.32(03)	1.85(37)			3, 18, 21
SN 2006 sr	NV	1.18(03)	1.38(06)	0.01(03)	0.58(12)	•••		3, 4, 11
SN 2007A	NV	1.08(02)	0.95(03)	0.14(03)	0.90(14)	•••		3, 4, 11, 21
SN 2007F	NV	1.11(03)	0.95(03)	-0.06(03)	0.65(17)	3.45(07)	2.66(05)	3, 4, 11
SN 2007af	NV	1.08(02)	1.16(03)	0.01(03)	0.31(08)	3.43(03)	2.61(03)	3, 4, 11, 21
		` /	` /				\ - /	. , , , -

Table 1 (Continued)

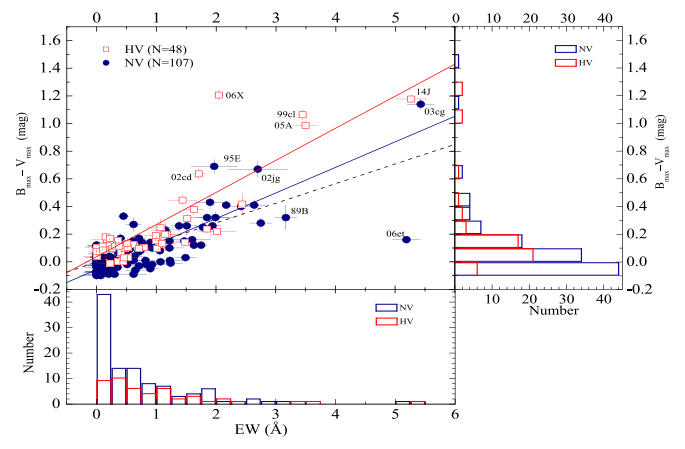
SN Name	SN Type	$(\times 10^{4}  \mathrm{km \ s^{-1}})$	$\Delta m_{15}(B)$ (mag)	$B_{ m max} - V_{ m max} \ ({ m mag})$	EW (Å)	$\Delta m_{60}(B)$ (mag)	$\Delta m_{60}(V)$ (mag)	References
SN 2007bc	NV	1.02(02)	1.29(05)	0.01(03)	0.62(19)	3.70(10)	2.90(05)	3, 4, 21
SN 2007bd	HV	1.24(05)	1.32(05)	-0.04(03)	0.45(09)	•••	•••	3, 4, 21
SN 2007bm	NV	1.05(05)	1.27(04)	0.41(03)	2.17(07)	•••	•••	3, 4, 11, 21
SN 2007ca	NV	1.05(03)	0.97(04)	0.26(03)	1.94(14)	3.40(06)	2.67(06)	3, 4, 11, 21
SN 2007ci	NV	1.17(02)	1.77(09)	0.04(03)	0.10(15)	•••	•••	3, 4, 10, 11
SN 2007co	NV	1.18(02)	1.13(05)	0.12(03)	0(16)			3, 4, 10
SN 2007cq	NV	1.05(03)	1.23(03)	-0.03(03)	0(14)	3.45(11)	2.68(08)	3, 4, 10, 11
SN 2007fb	NV	1.14(03)	1.39(05)	-0.09(03)	0.62(22)	3.65(05)	2.90(05)	3, 4, 23
SN 2007gi	HV	1.56(03)	1.37(05)	0.14(03)	0.23(10)	3.25(03)	2.70(03)	22
SN 2007hj	HV	1.20(02)	1.64(05)	0.12(03)	0.36(09)	3.62(14)	2.93(07)	4, 10, 22
SN 2007jg	HV	1.26(04)	1.22(03)	0.07(03)	0.52(10)	3.46(04)	2.87(04)	4, 22, 23
SN 2007kk SN 2007le	HV HV	1.25(05)	0.87(04)	-0.01(03)	0.53(19)	3.08(34)	2.40(15)	4, 23
		1.29(06)	1.02(05)	0.29(03)	1.52(06)	3.16(03)	2.56(02)	3, 4, 10, 23
SN 2007nq	NV	1.19(02)	1.54(04)	0(02) 0.05(03)	0(20)	3.63(05)	2.97(03)	4, 18, 21, 23
SN 2007qe SN 2007 sr	HV HV	1.35(05) 1.31(05)	0.98(03) 1.05(07)	0.08(03)	0.11(07) 0.31(12)	3.30(06) 3.20(03)	2.70(07) 2.57(02)	3, 4, 10, 11 4, 10, 16, 18
SN 2007 SI SN 2007ss	NV	1.18(03)	1.35(07)	0.28(04)	2.75(19)	3.55(10)	2.69(08)	4, 10, 10, 18
SN 2007ss SN 2007sw	HV	1.34(03)	1.04(05)	0.12(04)	1.00(13)	3.33(10) 	2.09(08)	4, 23
SN 2007sw SN 2007ux	NV	1.07(03)	1.53(08)	0.12(04)	0(15)	3.63(05)	2.95(04)	3, 4, 18
SN 2007ux SN 2008C	NV	1.06(03)	1.19(03)	0.11(03)	1.22(08)	3.03(03)	2.69(04)	4, 16, 18, 23
SN 2008Z	NV	1.12(03)	0.88(03)	0.10(03)	0.93(21)	3.30(05)	2.60(04)	3, 4, 23
SN 2008ar	NV	1.02(02)	1.09(03)	-0.02(03)	0(19)	3.38(03)	2.62(03)	3, 4, 10, 21
SN 2008bc	NV	1.16(03)	0.92(03)	-0.04(03)	0.35(07)	3.31(04)	2.63(02)	3, 4, 21
SN 2008bf	NV	1.13(02)	0.95(04)	-0.08(03)	0.08(15)	3.40(03)	2.64(03)	3, 4, 10, 11, 21
SN 2008bq	NV	1.05(02)	1.01(03)	0.09(02)	0.55(11)			18, 21
SN 2008dr	HV	1.44(03)	1.52(06)	0.08(03)	0.38(13)			3, 10
SN 2008ec	NV	1.10(02)	1.33(04)	0.15(03)	0.61(12)	3.62(10)	2.71(06)	3, 10
SN 2008fp	NV	1.12(03)	0.89(03)	0.40(03)	2.42(20)	3.30(03)	2.54(02)	18, 21
SN 2008fr	NV	1.04(04)	0.95(10)	-0.07(03)	0(20)	3.41(03)	2.46(03)	21, 23, 24
SN 2008gl	HV	1.20(03)	1.35(04)	0.03(03)	0(13)	3.46(04)	2.80(03)	18, 21
SN 2008gp	NV	1.06(02)	1.05(04)	-0.09(03)	0(14)			18, 21
SN 2008hv	NV	1.09(03)	1.21(05)	-0.07(03)	0(19)	3.50(02)	2.84(02)	18, 21, 23
SN 2008ia	NV	1.13(03)	1.31(05)	-0.02(03)	0.93(31)		•••	18, 21
SN 2009Y	HV	1.47(04)	0.97(03)	0.15(03)	0.15(05)	3.01(03)	2.51(02)	18, 21, 23
SN 2009aa	NV	1.05(03)	1.21(03)	-0.07(03)	0(19)	3.60(03)	2.71(03)	18, 21
SN 2009ab	NV	1.08(03)	1.22(04)	-0.02(03)	0.51(21)	•••	•••	18, 21
SN 2009ad	NV	1.03(02)	1.00(03)	-0.05(03)	0.90(15)	•••	•••	18, 21, 23
SN 2009ag	NV	1.02(02)	1.06(05)	0.17(03)	0.40(08)	•••	•••	18, 21
SN 2009ig	HV	1.30(03)	0.90(05)	0.07(03)	0.52(14)	3.05(03)	2.48(03)	3, 23
SN 2011fe	NV	1.04(02)	1.18(03)	-0.03(03)	0.07(05)	3.55(03)	2.65(03)	25
SN 2014J	HV	1.21(02)	0.98(02)	1.20(03)	5.27(26)	3.18(03)	2.44(02)	26, 27
				Peculiar 91T-like Subclass				
SN 1991T	91T	0.98(02)	0.94(03)	0.18(03)	1.30(14)	3.12(03)	2.43(03)	28, 29
SN 1995ac	91T	0.95(03)	0.83(05)	-0.01(05)	2.04(53)	3.16(04)	2.55(07)	4, 5
SN 1995bd	91T	0.96(03)	0.87(03)	0.42(03)	1.49(15)	3.05(04)	2.43(05)	4, 5
SN 1998ab	91T	1.00(04)	1.03(02)	0.07(03)	0.60(19)	3.45(05)	2.51(03)	4, 5
SN 1998es	91T	1.04(02)	0.78(03)	0.09(03)	1.36(12)	3.25(05)	2.38(04)	8, 10
SN 1999aa	91T	1.05(02)	0.81(02)	-0.01(02)	0.05(12)	3.20(07)	2.45(04)	8, 10
SN 1999ac	91T	1.00(03)	1.30(03)	0.09(03)	0.05(08)	3.38(02)	2.51(02)	7, 8, 10
SN 1999dq	91T	1.08(03)	0.90(03)	0.07(03)	1.00(07)	3.27(04)	2.46(03)	4, 6, 9
SN 1999gp	91T	1.10(03)	0.82(03)	0.04(03)	0.27(20)	•••	•••	4, 5, 8
SN 2000cx	91T	1.14(03)	0.98(03)	-0.10(03)	0(20)	3.52(03)	3.12(02)	3, 4, 8
SN 2001V	91T	1.13(03)	0.92(03)	-0.01(03)	1.26(11)	3.21(03)	2.45(03)	4, 5
SN 2001eh	91T	1.03(02)	0.78(03)	0.02(03)	0(20)	3.11(04)		3, 4
SN 2003fa	91T	1.03(03)	0.88(03)	-0.03(03)		3.62(08)	2.51(07)	4, 10
SN 2004bv	91T	0.71(03)	0.98(03)	0.10(04)	0.71(13)	3.22(06)	2.42(03)	3, 10
SN 2004br	91T	1.10(04)	0.87(03)	-0.04(03)	0(19)	•••	•••	3, 10
SN 2004gu	91T	1.14(02)	0.80(06)	0.13(03)	1.83(15)	2.21(02)	2.51(02)	16, 17, 18
SN 2005M	91T	0.81(03)	0.85(05)	-0.01(03)	0.25(13)	3.31(03)	2.51(03)	3, 10
SN 2005eq	91T	1.00(02)	0.78(03)	0.04(03)	0.75(17)	3.25(05)	2.52(02)	4, 11
SN 2005eu	91T	1.04(05)	0.87(03)	-0.08(03)	0.60(28)	•••	2.52(02)	3, 4, 10, 11
SN 20051s	91T	1.10(03)	0.95(10)	0.30(03)	1.81(36)	•••	2.52(03)	5, 6

Table 1 (Continued)

SN Name	SN Type	$(\times 10^{4}  \text{km s}^{-1})$	$\Delta m_{15}(B)$ (mag)	$B_{ m max} - V_{ m max} \  m (mag)$	EW (Å)	$\Delta m_{60}(B)$ (mag)	$\Delta m_{60}(V)$ (mag)	References
SN 2006cm	91T	1.10(02)	1.10(10)	0.94(04)	2.12(39)	•••	•••	4, 11
SN 2006mp	91T	0.81(03)	0.92(03)	-0.01(03)	0(20)	3.51(13)		4, 11
SN 2007S	91T	0.97(03)	0.89(03)	0.38(03)	1.70(18)	3.22(05)	2.38(03)	4, 11
SN 2007ai	91T	0.97(03)	0.90(03)	0.20(03)	1.46(26)	3.28(09)	2.55(05)	16, 18
SN 2007cq	91T	1.04(02)	1.14(09)	0.04(03)	•••	3.25(04)	•••	4, 11
				Peculiar 91bg-like Subclass				
SN 1991bg	91bg	1.02(02)	1.93(05)	0.75(05)		3.19(08)	•••	30
SN 1998bp	91bg	1.07(02)	1.83(05)	0.30(10)	0(14)	3.52(10)	3.02(05)	4, 7
SN 1998de	91bg	1.11(03)	1.96(05)	0.71(03)	0(30)	3.24(10)	3.06(10)	4, 10
SN 1999by	91bg	1.02(03)	1.91(05)	0.50(03)	0(20)	3.51(10)	3.20(10)	4, 8
SN 1999 da	91bg	1.13(02)	1.94(05)	0.68(05)	0(16)		•••	10
SN 2002cf	91bg	1.07(02)	1.86(10)	0.47(03)	•••		3.14(08)	3, 10
SN 2002dl	91bg	1.15(05)	1.85(03)	0.14(03)	0.54(17)	3.53(06)	2.94(05)	3, 4, 10
SN 2002fb	91bg	1.07(03)	1.88(05)	0.41(04)	0.31(11)	3.30(12)	3.17(10)	3, 4, 10
SN 2003gs	91bg	1.14(03)	1.93(07)	0.63(07)	•••	3.25(06)	3.15(07)	3, 10
SN 2005bl	91bg	0.98(02)	1.93(10)	0.78(03)	2.60(30)		3.16(17)	31
SN 2005ke	91bg	0.95(03)	1.81(04)	0.61(03)	0(10)	3.11(03)	3.07(04)	4, 16
SN 2005mz	91bg	1.07(05)	1.96(07)	0.33(07)		3.50(15)	3.26(07)	4, 11
SN 2006bz	91bg	1.09(03)	2.09(16)	0.70(08)	0.43(33)			4, 11
SN 2006em	91bg	1.03(03)	1.98(16)	0.89(10)	0(32)	•••		4, 11
SN 2008bt	91bg	0.98(03)	1.90(10)	0.47(03)		3.33(04)	3.00(05)	16, 18, 21

Note. The uncertainties shown in the brackets are  $1\sigma$ , in units of 0.01 mag for  $\Delta m_{15}(B)$ ,  $B_{\rm max} - V_{\rm max}$ ,  $\Delta m_{60}(B)$ , and  $\Delta m_{60}(V)$ , and in units of 0.01 Å for EW of Na I D absorption.

References. (1) = Barbon et al. (1989), (2) = Wells et al. (1994), (3) = Silverman et al. (2012), (4) = Blondin et al. (2012), (5) = Riess et al. (1999), (6) = Riess et al. (2005), (7) = Jha et al. (2006), (8) = Matheson et al. (2008), (9) = Jha et al. (1999), (10) = Ganeshelingam et al. (2010), (11) = Hicken et al. (2009), (12) = Kotak et al. (2005), (13) = Stanishev et al. (2007), (14) = Krisciunas et al. (2007), (15) = Altavilla et al. (2007), (16) = Contreras et al. (2010), Krisciunas et al. (2017), (17) = Pastorello et al. (2007), (18) = Folatelli et al. (2013), (19) = Wang et al. (2009b), (20) = Wang et al. (2008a), (21) = Stritzinger et al. (2011), Krisciunas et al. (2017), (22) = Zhang et al. (2010), (23) = Hicken et al. (2012), (24) = Yuan et al. (2008), (25) = Zhang et al. (2016), (26) = Brown et al. (2015), (27) = Zhang et al. (2018), (28) = Filippenko et al. (1992a), (29) = Lira et al. (1998), (30) = Filippenko et al. (1992b), (31) = Taubenberger et al. (2008). (This table is available in machine-readable form.)



**Figure 1.** Relation between absorption strength (expressed as equivalent width) of interstellar sodium lines in spectra of SNe Ia and the corresponding values of their  $B_{\rm max}-V_{\rm max}$  colors. The "HV" subgroup (red squares) represents the SNe Ia with larger Si II velocity at *B*-band maximum light, i.e.,  $v_{\rm Si~II}^0 > 12,000~{\rm km~s^{-1}}$ , while the "NV" subgroup (blue circles) denotes those with  $v_{\rm Si~II}^0 < 12,000~{\rm km~s^{-1}}$ . The red and blue lines represent the best-fit linear relationship to the HV and NV SNe Ia, respectively, while the dashed black line shows the relationship inferred from the Na absorption and reddening due to the Milky Way. SN 2006X was not included in the fit due to the saturation of the Na I lines (Patat et al. 2007) and SN 2006et appears to be an outlier and was not included in the fit either. The plot is then projected onto the two side panels, where a histogram is displayed for each SN Ia subclass in each of the dimensions.

26.2% for the NV counterparts). These results indicate that the HV SNe Ia suffer systematically larger reddening on average than the NV ones; the intrinsic color of HV SNe Ia may not necessarily be redder than their NV counterparts despite their observed red color, contrary to previous studies (i.e., Foley & Kasen 2011).

Applying a linear fit to the EW  $-(B_{\rm max}-V_{\rm max})$  relation for the HV and NV SNe Ia separately, we found that the former subclass has a larger slope of  $0.239\pm0.016$ , while the slope for the latter is  $0.177\pm0.011$ . This difference may be explained with incomplete recombination of the ionized Na (see Figure 2) and/or time evolving scattering of the SN photons by the surrounding dust (Wang 2005).

It is important to further constrain the location of the dust that gives rise to the excess extinction and the time-varying Na I D absorption in HV SNe Ia. If the SN exploded near a dusty shell/slab, we may expect variable Na I absorptions in SN spectra due to the photoionization effect (Chugai 2008; Patat et al. 2011). The strength of the absorption may then be correlated with the rise and fall of the supernova luminosity. The trend in which the Na I D absorptions become stronger after maximum light has already been reported for a few SNe Ia such as SN 2006X (Patat et al. 2007), SN 2007le (Simon et al. 2009), and SN 1999cl (Blondin et al. 2009), but the decrease in strength of Na I absorption expected shortly after explosion was never observed in SNe Ia.

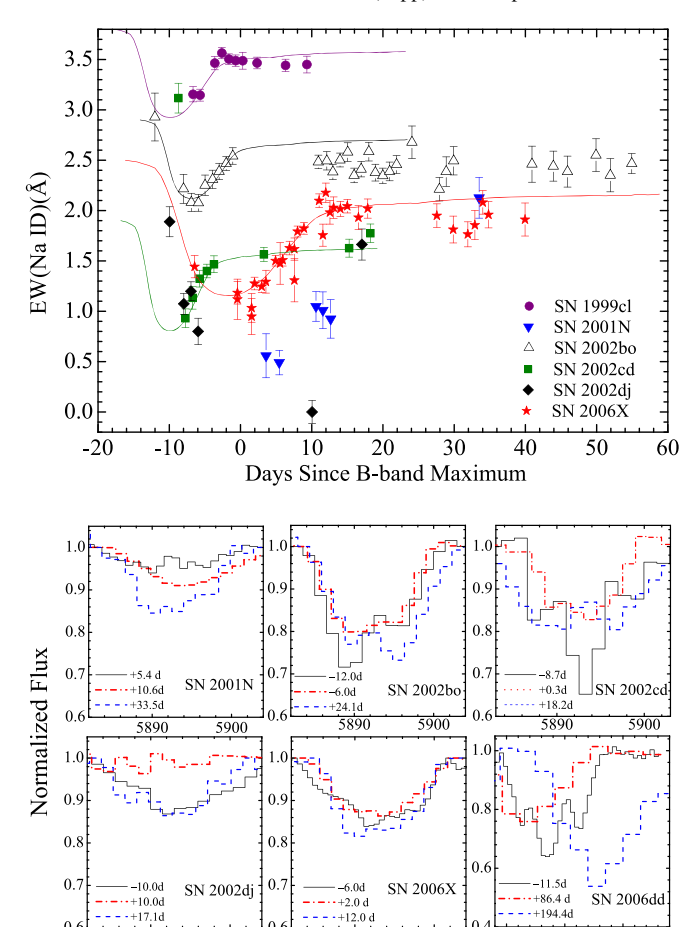


Figure 2. Temporal evolution of the equivalent width of the Na I doublet for SNe Ia. Top panels: variable Na absorptions detected in some well-observed objects such as SNe 1999cl, 2001N, 2002bo, 2002cd, 2002dj, and 2006X. Note that all of the six SNe Ia shown in the plot belong to the "HV" subclass. Overplotted are the curves derived with a model of Na I photoionization and recombination in CS dust. Bottom: the continuum-normalized Na I D profile shown at several epochs for some well-observed HV SNe Ia. The black and red lines represent the earlier and near-maximum-light phase spectra, respectively, while the blue ones show the profile in the recombination phase.

+12.0 d

5890

SN 2006X

Rest-frame Wavelength[Å]

0.4 5880

5890

SN 2006dd

SN 2002dj

5900

To investigate the EW variations, we consider all objects having at least three epochs of spectroscopic data within  $\sim$ 1 month from the maximum light. Applying a  $3\sigma$  detection cut and a minimum EW variation of 0.5 Å to the CfA and CSP data, we get a sample of 16 SNe Ia showing prominent Na I D variations. Table 2 lists the relevant parameters of this sample showing variable Na absorptions. Of these 16 SNe Ia, there are 11 HV and 2 NV SNe Ia, with a fraction of 68.8% and 12.5%, respectively. This sample increases to 23 when applying a  $2\sigma$ cut, which contains 13 HV SNe Ia (56.5%) and 6 NV SNe Ia (26.0%). The above analysis indicates that the varying of Na I D absorptions are statistically associated with the HV subclass. The probability of a chance coincidence is less than 0.1%. Variable sodium features have already been detected in the high-resolution spectra of SN 2006X and SN 2007le, and lowresolution spectra of SN 1999cl. It is gratifying to note that the evolutions of their Na I D lines are nicely recovered in these low-resolution data.

Note that SN 2006dd was also proposed as an SN Ia showing significant changes in the Na I D absorptions (Stritzinger et al. 2010) and is thus listed in Table 2. Its EW of Na I D absorption

seems to decrease from  $\sim$ 3.2 Å at  $t \sim -12$  and  $t \sim +86$  days to  $\sim 1.3 \,\text{Å}$  at  $t \sim +137$  days and then increase to  $\sim 3.8 \,\text{Å}$  at +194 days. Owing to the lack of near-maximum-light spectra, we cannot put this object into the HV or NV subclasses. We caution, however, that the center wavelength of the absorption features around 5890 Å in the spectra of SN 2006dd changes from  $5884 \,\text{Å}$  in the  $+86.4 \,\text{day}$  spectrum to  $5896 \,\text{Å}$  in the  $t \sim +194.4 \,\mathrm{day}$  spectrum. Such a large change may indicate improper wavelength calibration, or the identified "Na I" absorption might actually be caused by other unknown features given that this SN has relatively blue B - V color.

The Na I D absorption of some representative SNe Ia with significant time evolution is shown in Figure 2. The plot suggests that the Na I D lines of these objects generally follow a qualitatively similar evolutionary trend. At early times the strength of the Na I D absorption was found to decrease with time, as is clearly seen in SN 2002bo, SN 2002dj, SN 2006X, and perhaps in SN 2002cd. Such evolution can be attributed to photoionization of neutral Na by the UV photons of supernovae (Borkowski et al. 2009). After the declining phase, the Na absorption strength undergoes a rising stage lasting for about 10 days and remains at a constant level after that. The overall evolution looks like a "square-root" sign, which can be explained with a model of Na I D photoionization and recombination in CS dust (see the solid curves in Figure 2) as discussed in Section 3.3.

## 3.2. Late-time Light Curves

The presence of CS dust can be also tested by examining the behaviors of the late-time light curves of SNe Ia. This is because some of the SN photons will be scattered by surrounding dust and arrive at the observer with a time delay (Wang & Wheeler 1996; Wang 2005; Patat et al. 2006). The delayed photons can be seen as a light echo (LE) and may contribute to the observed light curves in the early nebular phase, especially in blue bands. To examine the differences in the late-time light curves for our sample of SNe Ia, we measured the magnitude decline within 60 days from the *B*-band and *V*-band maximum light, as defined by  $\Delta m_{60}(B)$  and  $\Delta m_{15}(V)$ , respectively. These two quantities are obtained by applying a linear fit to the observed data spanning the phase from  $t \sim +40$  days to  $t \sim 100$  days, as listed in Table 1.

Figure 3 shows the BV-band light curves and the B - Vcolor curves for some well-observed SNe Ia. Although these SNe Ia have similar light curves in early phases, they show remarkable scatter in the *B*-band from  $t \sim 40$  to 100 days after the peak. For instance, the B-band magnitude measured at  $t \sim 60$  days from the peak can differ by over 0.5 mag in the B band (see Figure 3(a)). This late-time discrepancy is much smaller in the V band (see Figure 3(b)), which leads to an apparently bluer B - V color for the HV SNe Ia relative to the NV objects, as shown in the right panel of Figure 3.

As more luminous SNe Ia tend to have brighter tails with slower decay rates, it is thus necessary to examine whether the excess emission seen in the tail light curves of HV SNe Ia is partially due to them having intrinsically high luminosity. We plot the measured values of  $\Delta m_{60}$  as a function of the corresponding  $\Delta m_{15}(B)$  for our sample in Figure 4, where one can see that the tail brightness shows a significant correlation with the decline rate in both the B and V bands for the NV sample of SNe Ia. While this correlation shows large scatter in the B band for the HV subsample, the measured  $\Delta m_{60}(B)$  is

 Table 2

 Candidates of Type Ia Supernovae with Variable Na I D Absorption Features

SN Name	$\Delta \text{EW}(\mathring{A})^{a}$	$\Delta \mathrm{EW}/\sigma^{\mathrm{b}}$	Number <sup>c</sup>	Phase of the Spectra (days) <sup>d</sup>	Type
SN 1997bp	0.66	3.5	13	-1.6, 2.3, +20.3, +33.2, +51.2	HV
SN 1997bq	0.96	4.7	8	-10.6, -4.5, +12.4, +20.4	HV
SN 1999cl	1.07	5.0	11	-6.7, -2.6, +9.3, +39.3	HV
SN 1999dq	0.73	3.8	21	-9.5, -3.5, 30.3, +59.3, +90.3	91T
SN 2001br	1.27	4.4	4	-1.1, +1.9, +26.9, +53.8	HV
SN 2001N	1.64	6.9	6	+3.6, +10.6, +12, 7, +33.5	HV
SN 2002bf	1.38	4.7	4	+3.8, +6.8, +8.8, +12.8	HV
SN 2002bo	0.85	3.4	31	-12.0, -5.9, -1.1, +11.0, +22.0	HV
SN 2002cd	2.19	12.5	9	-8.7, -4.7, +0.3, +15.2,	HV
SN 2002dj	1.89	10.0	6	-10.0, -5.9, +10.1, +17.1	HV
SN 2003ep	2.23	10.6	3	a few weeks later	
SN 2005hf	1.10	3.9	6	+3.0, +7.0, +13.1	Pec
SN 2006N	1.02	4.1	7	+2.2, +5.2, +8.2, +28.2	NV
SN 2006X	0.93	8.2	21	-6.6, +3.0, +8.0, +15.0, +34.0	HV
SN 2006dd	2.53	3.7	5	-12.0, +86.4, +137.0, +194.4	
SN 2007le	0.67	4.0	25	-6.3, +5.6, +19.6, +40.5, +67.6	HV
SN 2008C	1.27	6.5	5	+9.5, +13.5, +30.5, +43.5	NV

#### Notes.

systematically smaller than that of the NV ones at a given  $\Delta m_{15}(B)$ . This comparison further confirms that the excess emission in the blue band is not intrinsic to the HV SNe Ia. Instead, we found that the  $\Delta m_{60}(B)$  shows a strong positive correlation with the Si II 6355 velocity measured around the maximum light, as shown in Figure 4(c). This indicates that the origin of the larger expanding velocity might be closely related to the formation of dusty environments around SNe Ia, and hence the properties of the progenitor system.

## 3.3. Modeling of the Observed Results

In this subsection, we explore the presence of CS dust and constrain its distance from the SNe by comparing the modeling results with both the variations of Na I D absorption observed in the spectra and the excess emission detected in the late-time light curves.

## 3.3.1. Photoionization Model

To study the effect of photoionization on the observed Na I absorptions in SN Ia spectra, we consider a simple model with a spherical CS dust shell. Similar models have been employed in previous studies (Patat et al. 2007; Borkowski et al. 2009) to study the variations in Na absorption lines, but only the recombination process was emphasized. The Na ionization state is actually determined by the balance between ionizations and recombinations. In our calculations, both of these stages are explored based on the change of the ionization and recombination rates with the ultraviolet flux emitted by the SNe Ia at different phases. We assume that the pre-explosion number of Na I in the CS shell is  $N(\text{Na I})(t_0)$  well before the SN explosion, and the change of this number over a time span dt

can be written as

$$dN(\text{Na I})(t)/dt = \frac{dN(\text{Na I})_{\text{ion}}(t) + dN(\text{Na I})_{\text{rec}}(t)}{dt}$$

$$= -N(\text{Na I})(t_0) \cdot R_{\text{ion}}(t) + [N(\text{Na I}) - N(\text{Na I})(t)] \cdot R_{\text{rec}}(t)$$
(1)

 $R_{\rm ion}(t)$  and  $R_{\rm rec}(t)$  represent the ionization rate of Na I and recombination rate of Na II, respectively. Defining the fraction of Na I as  ${\rm Frac}({\rm Na\,I}(t)) = \frac{N({\rm Na\,I})(t)}{N({\rm Na\,I})(t_0)}$  and inserting it into the above equation, we can derive a differential equation as

$$\frac{d\operatorname{Frac}(\operatorname{Na}\operatorname{I})(t)}{dt} + \left[R_{\operatorname{ion}}(t) + R_{\operatorname{rec}}(t)\right] \cdot \operatorname{Frac}(\operatorname{Na}\operatorname{I})(t) - R_{\operatorname{rec}}(t) = 0. \tag{2}$$

This has the following solution:

Frac(Na I)(t) = 
$$\exp\{\int_{t_{\exp}}^{t} -[R_{\text{ion}}(t') + R_{\text{rec}}(t')]dt'\}$$
  
  $\times \{\int_{t}^{t} e^{\int_{t_{\exp}}^{t'} [R_{\text{ion}}(t'') + R_{\text{rec}}(t'')]dt''} \cdot R_{\text{rec}}(t')dt' + 1\}.$  (3)

According to photoionization theory, the ionization rate and recombination rate can be expressed as

$$R_{\text{ion}}(t) = \sigma \cdot I(t);$$
  

$$R_{\text{rec}}(t) = \alpha(T_e(t)) \cdot n_e(t).$$
 (4)

Here,  $\sigma$  is the photoionization cross section of Na I and I(t) is the photon count rate per unit area. The photoionization cross section depends on the energy of the incoming photons, and only the photons with energy higher than 5.139 eV can remove the electrons from the ground state for Na I (Verner et al. 1996). In other words, the photons responsible for Na ionizations should have a wavelength shorter than 2412 Å. Here we adopted the spectral template of SNe Ia (Nugent et al. 2002; Hsiao et al. 2007)

a The maximum variation of the equivalent width (EW) measured from the Na I absorption in the spectra of SNe Ia.

b The confidence that the SNe Ia show variable Na I D absorption, obtained by dividing the maximum variation of EW over the uncertainty in the measurement.

<sup>&</sup>lt;sup>c</sup> The number of spectra used in the analysis.

d Relative to the B-band maximum, and only the representative phases are shown for the limited space.

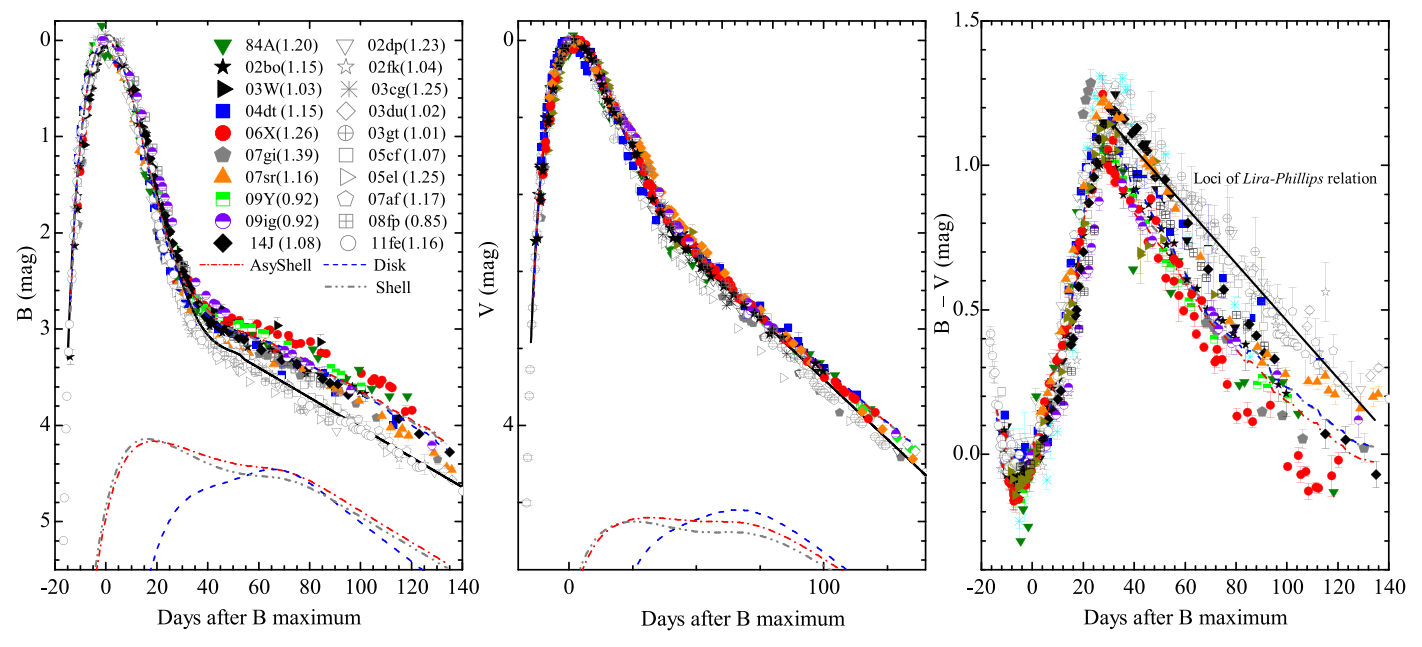


Figure 3. The *B*-band light curve (left panel), *V*-band light curve (middle panel) and B-V color curve (right panel) of some well-observed SNe Ia (see Table 1 for the references of the data), with all the curves normalized to the corresponding values at around the maximum light. The filled and semi-filled symbols represent the HV SNe Ia, and the open symbols denote the NV SNe Ia. The SNe Ia of these two subclasses exhibit large differences in *B* band and B-V colors 40 days after the maximum brightness. The black solid lines indicate the mean light curves of the NV subsample. The extra emission from scattering of SN light onto CS materials of a spherical shell, asymmetric shell, and a disk structure, at a distance of  $\sim 1-2 \times 10^{17}$  cm, are shown with the gray dashed—dotted, red dashed—dotted, and blue dashed lines, respectively. The resultant light curves from including contributions of CS scattering are indicated with the same symbols. The black solid line shows the best fit to the B-V color curves of NV SNe Ia using the updated Lira–Phillips relation (Burns et al. 2014), with the non-reddening loci shifted redward by 0.2 mag. For the interval of 40 days < t < 100 days, the color curves of most HV SNe Ia are apparently bluer than those of normal SNe Ia, following a slope much steeper than the Lira–Phillips relation.

to generate the UV photons needed to ionize Na I. The UV flux has been scaled to the peak luminosity of SNe Ia with Cepheid distances (Riess et al. 2016) and is then converted into photon count rate. Meanwhile, the second equation of Equation (4) shows that the recombination rate of Na II is related to the recombination coefficient  $\alpha(T_e(t))$  (which can change with the temperature T) and electron density within the CS shell  $n_e(t)$ . We simply assume a constant temperature and electron density in our model by adopting them as the mean values of these two parameters. Then the recombination rate can be expressed as  $R_{\rm rec} = \alpha(T_e) \cdot n_e$ . Following the literature (i.e., Douvion et al. 2001; Kamp & Van Zadelhoff 2001; Johansson et al. 2013), we adopt a typical temperature of 100 K for the CS dust. And the relationship between  $\alpha$  and  $T_e$  is determined by Verner & Ferland (1996).

Some model curves from our calculations, adjusted for the observed data of some SNe Ia in our sample, are shown in Figure 2. The overall evolution of Na I D absorption seen in some HV SNe Ia is similar to that predicted by a simple CS shell model (see the solid curves in Figure 2). By comparing with the model curves, typical values of  $R_S \sim 0.1 \, \mathrm{pc}$  (3 × 10<sup>17</sup> cm) and  $n_e \sim 5 \times 10^7 \, \mathrm{cm}^{-3}$  can be found for the subsample showing evolving Na I D absorptions. Of the sample listed in Table 2, the reddening toward SN 2001N may be dominated by the CS dust, as Na seems to be nearly completely ionized around the peak luminosity and the dust shell may be located at a distance of  $R_S < 0.1$  pc. The longer recombination timescale ( $\gtrsim$ 30 days) suggests that the density of the CS material is quite low, e.g.,  $n_e \ (\lesssim 10^7 \, \mathrm{cm}^{-3})$ . Note that estimates of the above parameters may suffer large uncertainties due to the difficulty of distinguishing the CS component from the component of Na I D absorption in these low-resolution spectra. Moreover, it is also difficult to determine accurately the total amount of neutral Na due to line saturation. Nevertheless, the above analysis indicates that the excess reddening of HV SNe Ia is related to the CS dust.

## 3.3.2. Dust Scattering Model

The dust scattering process can be implemented with an elastic scattering (including Rayleigh scattering and Mie scattering). Light scattering in the circumstellar environments of SNe Ia was first studied by Wang (2005), who found that the inclusion of the scattered light tends to reduce the total extinction and hence the ratio of extinction to color excess, i.e.,  $R_V = A_V/E(B - V)$ . This provides an alternative explanation for the unusually low  $R_V$  observed in some SNe Ia. Later on, Goobar (2008) conducted a similar study by considering the effects of both scattering and absorption (due to a CS shell) on the SN light. Multiple scattering processes will predominately attenuate photons with shorter wavelengths, thus steepening the effective extinction law. Moreover, such a light scattering can be observed as an LE phenomenon at late time when the SN light becomes faint enough. As blue photons usually scatter more for dust grains with smaller size, the resulting echo would thus appear blue. However, after multiple scattering, the blue photons could finally be absorbed or directed off the line of sight for some specific optical depth, while the red photons suffer less scattering and absorption. And this contrast will lead to the production of a red echo.

The extra light seen in the *B*-band light curves of the HV SNe Ia shown in Figure 3 could be due to the scattering of SN light by the nearby CS dust, which can be quantitatively modeled for any given geometric configuration. In our models of dust scattering, we adopt Mie scattering and consider three structures of CS dust: a spherical shell, an asymmetric shell

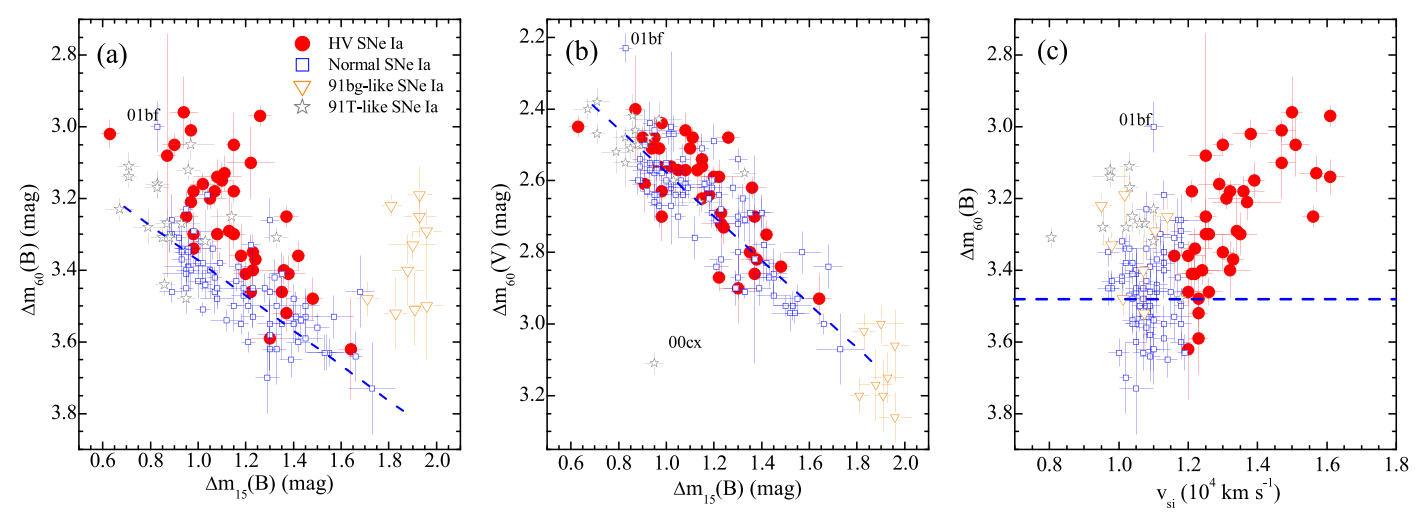


Figure 4. (a) and (b): tail brightness of SNe Ia, measured as magnitude decline at  $t \sim +60$  days from the peaks of *B*-band and *V*-band light curves, vs. the luminosity indicator of SNe Ia  $\Delta m_{15}(B)$  that is measured as the magnitude decline within the first 15 days after the *B*-band maximum (Phillips 1993). (c): plot of the *B*-band tail brightness as a function of the Si II velocity obtained around *B*-band maximum light. The SNe Ia subclasses of HV, NV, and spectroscopically peculiar objects like SN 1991T and SN 1991bg SNe are shown by blue open squares, red dots, gray stars, and orange triangles, respectively. The blue dashed line in each panel represents the best linear fit for the NV subsample.

(AsyShell), and a disk configuration, as shown in Figure 5. There are more complicated configurations, such as tori or blobs, but these discussions will be presented in a forthcoming paper (M. K. Hu et al. 2019, in preparation).

For the spherical shell and disk structures, the number density of dust grains along the radial direction (N(R)) is assumed to decrease inversely with radius squared, i.e.,  $A/R^2$ , where R is the distance to the SN and A relates to the optical depth. Thus, three parameters,  $R_{\text{inner}}$  (inner radius of the shell),  $R_{\text{outer}}$  (outer radius of the shell), and  $\tau$  (optical depth), can be used to define the geometric property of the shell structure. For the asymmetric shell, however, we consider additional dependence of the dust density on the angle from the symmetry axis  $\theta$ , with  $N(R, \theta) = A/R^2 \times (1 + (\sin^n \theta - 1)s)$ , where n and s describe degrees of asymmetry relative to the spherical shell and their best-fit values are 2.0 and 0.6, respectively. This modified relation can be regarded as an extended form of the number density given in Chevalier (1986). For the disk structure, an opening angle parameter  $\theta_{disk}$  is needed to address the thickness of the disk. Moreover, an observing angle  $\theta_{obs}$ needs to be assumed for both the disk and AsyShell structures.

In our calculations of the dust scattering, all the values of albedo  $(=\sigma_s/(\sigma_s+\sigma_a))$ , absorption cross section  $(\sigma_{abs})$ , scattering cross section  $(\sigma_{sca})$ , and phase function related to the scattering process are taken from Draine (2003). The size distribution of dust grains is adopted as

$$f(r) = r^{-a_0} \exp\left\{-b_0 \left(\log \frac{r}{r_0}\right)^{2.0}\right\},$$
 (5)

where  $a_0$  and  $b_0$  are adopted as 4.0 and 7.5, respectively, to be consistent with the results derived in Nozawa et al. (2015).

The modeled light/color curves, obtained by taking the mean light curves of NV SNe Ia as the input of light scattering, are overplotted in Figure 3. To match the observed *B*-band and *V*-band light curves of our HV sample, the CS dust is required to have an inner radius of  $R_{\rm inner} \sim 1 \times 10^{17}\,{\rm cm}$  and an outer radius of  $R_{\rm outer} \sim 2 \times 10^{17}\,{\rm cm}$  for most of our HV sample, with the optical depth  $\tau$  being about 0.12, 0.15, and 0.7 for the CS dust of the spherical shell, asymmetric shell, and disk

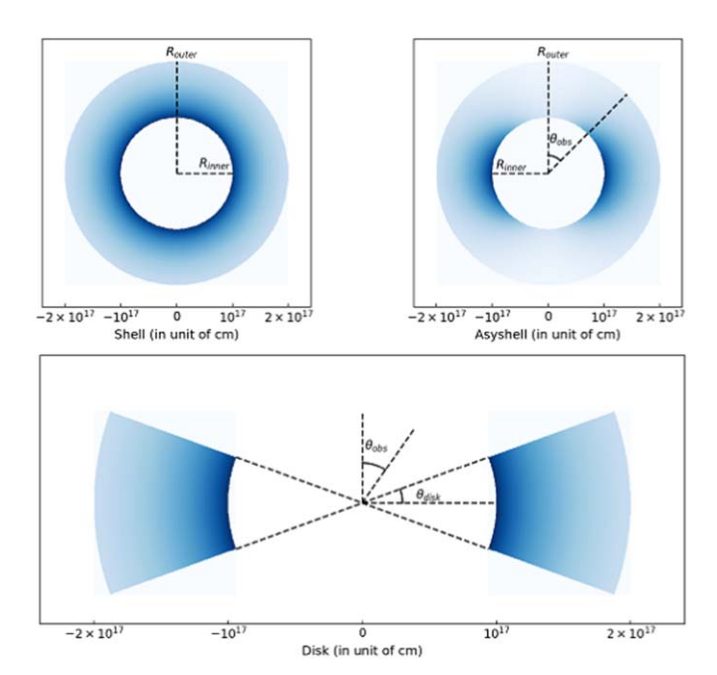


**Figure 5.** Illustration of the vertical planes of three different structures of CS dust, spherical shell (top left), asymmetric (top right), and the disk (bottom). The vertical dashed lines show the symmetry axes of the dust distribution.  $\theta_{\rm obs}$  shows the direction to the observer. The structures are rotationally symmetric with respect to the vertical dashed lines. The boundaries of the CSM are identified by the inner radius ( $R_{\rm inner}$ ) and the outer radius ( $R_{\rm outer}$ ). The grayscale indicates the number density of the dust grains. The dust density decreases inversely with radius squared in both cases. For (a), the azimuth density dependence follows  $\sin^2\theta$ , with  $\theta$  being the angle to the symmetry axis.

structures, respectively. The best-fit opening angle for the disk structure is  $\theta_{\rm disk} \sim 20^{\circ}$ . For the CS dust of asymmetric shell and disk structures, the symmetry axes are tilted at an angle  $\theta_{\rm obs} \sim 30^{\circ}$  with respect to the observer. Note that the results listed for the above parameters represent their average values because there are many sets of parameter values that can give reasonable fits to the light curves. The corresponding mass-loss rate of the stellar wind  $\dot{M}_w$  is estimated as  $\sim 9 \times 10^{-7} \, M_{\odot} \, {\rm yr}^{-1}$ ,  $\sim 8 \times 10^{-7} \, M_{\odot} \, {\rm yr}^{-1}$ , and  $\sim 6 \times 10^{-6} \, M_{\odot} \, {\rm yr}^{-1}$  for the CS dust

of shell, AsyShell, and disk structures, respectively. The calculation of  $\dot{M}_w$  is based on the equation of  $N = A/R^2 = \dot{M}_w/(4\pi v_w R^2 m)$ , where m is the average mass of each dust grain.

It is remarkable that the model light curves of different geometric configurations agree with the observed light/color scatter seen at 40–100 days after optical maximum. Note that the color measurements at these dates correspond to those used in the Lira–Phillips relation (Lira et al. 1998) for color excess estimates of SNe Ia. This agreement is encouraging and suggestive of the validity of these models, favoring the presence of CS dust around SNe Ia. Moreover, the distance of the CS dust inferred from modeling of the late-time light curve is in strikingly consistent with that derived from the photoionization calculations presented in Section 3.3.1. Further distinguishing between different geometric structures of the CS dust requires polarimetric observations at late time (see more discussions below).

We note that Bulla et al. (2018a, 2018b) also estimated the dust locations of SNe Ia from their B - V color evolutions. They simulated the propagation of Monte Carlo photons through a dust region and constrained the dust distances to their SN Ia sample at  $4 \times 10^{16}$ – $10^{20}$  cm, which is on average larger than our estimates. This difference is likely related to the dust properties adopted in the analysis. In the Bulla et al. analysis they chose the Milky Way-type dust and adopt a thin disk without an extended structure, while we adopt three different structures of CS dust with an average dust size of  $0.5 \mu m$ . A smaller dust grain is also favored for those SNe Ia with unusually low  $R_V$  (Goobar 2008; Wang et al. 2008b). In addition, the derived color excess E(B-V) from the B-Vcolor may suffer relatively large uncertainties due to larger photometric errors and some SNe Ia may have peculiar color evolution.

## 4. Discussions and Conclusions

The formation of nearby CSM around an SN progenitor is a direct consequence of its progenitor evolution. The CSM can be ejected continuously similar to stellar winds, or episodically similar to nova shell ejections. Typical blueshift in the Na I lines of SNe Ia is  $\sim 100$  km s<sup>-1</sup> according to a statistical study using high- and intermediate-resolution spectra of a large sample of SNe Ia (Sternberg et al. 2011; Maguire et al. 2013). The velocity and distance of the CS dust inferred here for HV SNe Ia suggest that they may have symbiotic nova progenitors, similar to RS Ophiuchi (Patat et al. 2011). Theoretical expectations for the fraction of SNe Ia from the symbiotic progenitor channel are  $\sim$ 1% to 30% (Lu et al. 2009), which is consistent with the birthrate of HV subclass, with a fraction of about 20% of all SNe Ia (Li et al. 2011b; Pan et al. 2015). For such a system, the fast-expanding nova shell (with a velocity of a few thousands of km s<sup>-1</sup>) ejected from recurrent nova outbursts will be slowed down by the slow-moving stellar wind blown from the companion star, i.e., a red giant. Such an interaction process can create a large evacuated region around the SN progenitor and form a CS shell with a velocity of  $\sim 100 \,\mathrm{km \, s^{-1}}$  at a distance ranging from  $10^{15}$  to  $10^{18} \,\mathrm{cm}$ , consistent with the estimates for the HV sample. The extension and distance of the CS dust from the progenitor are likely related to the accretion rate, period of recurrent nova, and the time lag between the explosion and mass loss before explosion.

The distribution of the CS dust derived for the HV SNe Ia is typically around 10<sup>17</sup> cm according to the above analysis,

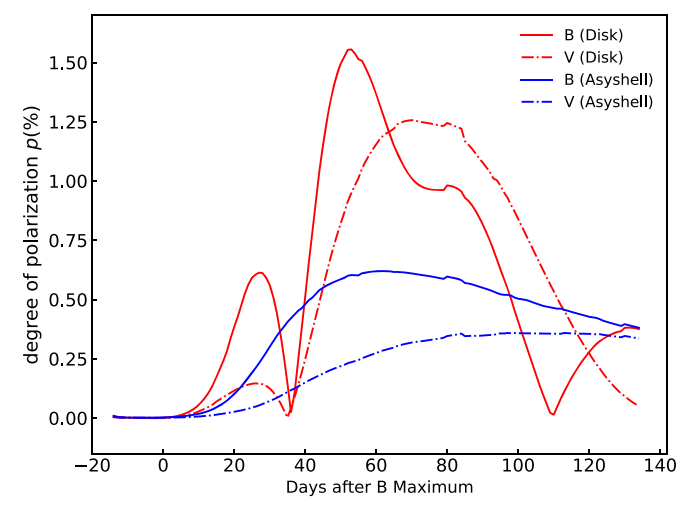


**Figure 6.** Predicted time evolution of the polarization in the B (solid line) and V bands (dotted–dashed line) at a viewing angle of  $30^{\circ}$  for the asymmetric shell. The blue curves show the polarization inferred from the asymmetric shell, while the red ones represent the case for the disk structure.

which is too compact to be spatially resolvable at extragalactic distances. The progenitors of SNe Ia involve binaries with one or two degenerate stars, the dust ejected from such systems may be naturally asymmetric. Polarimetry study of such compact light echoes is able to map the geometric structures of the CSM and set observational constraints on the progenitor systems. We remark that the asymmetric dust distribution naturally leads to polarized radiation at late times when the scattered light is the strongest, corresponding to about 60-90 days after optical maximum, as shown in Figure 6. The absolute level of the degree of polarization is sensitive to the assumed geometric structure. Although only the SNe with highly asymmetric CS dust shells close to being edge-on are expected to produce strong polarization, the detection of such polarized signal and its evolution can be prime evidence for the presence of the CS matter around the SNe (Wang & Wheeler 1996). Unfortunately, existing polarimetry data are mostly taken around optical maximum (Wang & Wheeler 2008). Indeed, recent deep HST imaging polarimetry of SN 2014J taken on day 277 after maximum reveals an abnormal polarization signal that can be identified with a light echo from a dust lump of at least  $2 \times 10^{-6} M_{\odot}$ , located at a distance of  $5 \times 10^{17}$  cm (Yang et al. 2018). More polarimetry at late epochs, coupled with photometric monitoring, holds the key to unlocking of the mystery of the CSM around SN Ia progenitors.

Our studies demonstrate that the HV SNe Ia are associated with the CS dust, which is in accordance with the detection of systematically blueshifted velocity structure (or outflow) in the Na I lines of SNe Ia having high Si II velocity (Sternberg et al. 2011). There is much additional evidence favoring the HV subclass as the origin of the single-degenerate progenitor system. For example, a significant ultraviolet excess is possibly detected in SN 2004dt and SN 2009gi (Wang et al. 2012; Foley & Kirshner 2013), which is expected from the collision between ejecta and a larger companion such as a massive MS star or a red giant star (Kasen 2010). Moreover, there is a tendency for unburned carbon (i.e., C II 6580 Å) to be detected in the earlier spectra of NV SNe Ia (Parrent et al. 2011; Blondin et al. 2012; Silverman et al. 2012), but not in the HV SNe Ia. Recent studies also indicate that these two subclasses of SNe Ia

show significant differences in the velocity distribution of outer-layer oxygen and silicon (Zhao et al. 2016). Moreover, detailed analysis of the late-time luminosity evolution of SN 2014J (a member of the HV subclass, see Zhang et al. 2018) suggests that the delayed-detonation model through the SD channel is the most favorable scenario for this SN Ia (Li et al. 2019). These results are in line with the idea that SNe Ia with different ejecta velocities have different progenitor systems and/or explosion mechanisms. Combined with the results from the evolving narrow interstellar Na I absorptions and the late-time light curves presented in this report, we suggest that SNe Ia with fast-expanding ejecta likely arise from progenitor systems with a red giant companion.

Nevertheless, some secular merger models may produce blueshifted absorbing materials, i.e., through interaction of tidal disrupted ejecta with the interstellar medium (Raski & Kasen 2013) or wind blown from the accretion disk (Dragulin & Hoeflich 2016). However, the former can only produce an absorbing shell with a blueshifted velocity of about 100 km s<sup>-1</sup>, after the ejection of a tidal tail for about 10<sup>4</sup> years when the absorbing materials moved to a distance of about 10<sup>18</sup> cm. In contrast, the fast wind from the accretion disk (with a velocity of  $\sim 3000 \, \mathrm{km \, s}^{-1}$ ) tends to produce a low-density void region several light years across, surrounded by a dense shell at a distance  $\gtrsim 10^{18}$  cm (Dragulin & Hoeflich 2016). Thus, neither of these two merger models could produce the CSM consistent with our result. Moreover, the core-degenerate (CD) scenario, an explosion of a WD and the core of an AGB star, has also been proposed as an alternative way to explain the presence of CSM around some SNe Ia (i.e., Soker 2015; Tsebrenko & Soker 2015), but it is not clear whether the observed properties of a CD SN Ia would resemble that of a typical SN Ia.

We thank the anonymous referee for the suggestive comments, which improved the manuscript. This work is supported by the National Natural Science Foundation of China (NSFC grants 11325313, 11633002, and 11761141001), and the National Program on Key Research and Development Project (grant No. 2016YFA0400803). The work of L.W. is supported by NSF grant AST-1817099. This research has made use of the CfA Supernova Archive, which is funded in part by the National Science Foundation through grant AST 0907903. This research has also made use of the supernova archives from the Carnegie Supernova Project and the Berkeley Supernova Program, which are also funded in part by the US National Science Foundation.

## **ORCID iDs**

Xiaofeng Wang https://orcid.org/0000-0002-7334-2357

### References

```
Aldering, G., Antilogus, P., Bailey, S., et al. 2006, ApJ, 650, 510
Altavilla, G., Stehle, M., Ruiz-Lapuente, P., et al. 2007, A&A, 475, 585
Barbon, R., Benetti, S., Cappellaro, E., Rosino, L., & Turatto, M. 1990, A&A, 237, 79
Barbon, R., Iijima, T., & Rosino, L. 1989, A&A, 220, 83
Blondin, S., Matheson, T., Kirshner, R. P., et al. 2012, AJ, 143, 126
Blondin, S., Prieto, J. L., Patat, F., et al. 2009, ApJ, 693, 207
Bochenek, C. D., Dwarkadas, V. V., Silverman, J. M., et al. 2018, MNRAS, 473, 336
Borkowski, K. J., Blondin, J. M., & Reynolds, S. P. 2009, ApJL, 699, L64
```

```
Branch, D., Fisher, A., & Nugent, P. 1993, AJ, 106, 2383
Brown, P. J., Smitka, M. T., Wang, L., et al. 2015, ApJ, 805, 74
Bulla, M., Goobar, A., Amanullah, R., Feindt, U., & Ferretti, R. 2018a,
           5, 473, 1918
Bulla, M., Goobar, A., & Dhawan, S. 2018b, MNRAS, 479, 3663
Burns, C. R., Stritzinger, M., Phillips, M. M., et al. 2014, ApJ, 789, 32
Chevalier, R. A. 1986, ApJ, 308, 225
Chugai, N. N. 2008, AstL, 34, 389
Contreras, C., Hamuy, M., Phillips, M. M., et al. 2010, AJ, 139, 519
Dilday, B., Howell, D. A., Cenko, S. B., et al. 2012, Sci, 337, 942
Douvion, T., Lagage, P. O., Cesarsky, C. J., & Dwek, E. 2001, A&A, 373, 281
Dragulin, P., & Hoeflich, P. 2016, ApJ, 818, 26
Draine, B. T. 2003, ApJ, 598, 1017
Filippenko, A. V., Richmond, M. W., Branch, D., et al. 1992b, AJ, 104, 1543
Filippenko, A. V., Richmond, M. W., Matheson, T., et al. 1992a, ApJL,
   384, L15
Folatelli, G., Morrell, N., Phillips, M. M., et al. 2013, ApJ, 773, 53
Folatelli, G., Phillips, M. M., Burns, C. R., et al. 2010, AJ, 139, 120
Foley, R. J., & Kasen, D. 2011, ApJ, 729, 55
Foley, R. J., & Kirshner, R. P. 2013, ApJL, 769, L1
Ganeshalingam, M., Li, W., Filippenko, A. V., et al. 2010, ApJS, 190, 418
Gilfanov, M., & Bogdán, Á. 2010, Natur, 463, 924
González-Hernández, J. I., Ruiz-Lapuente, P., Tabernero, H. M., et al. 2012,
Goobar, A. 2008, ApJL, 686, 103
Guy, J., Astier, P., Baumont, S., et al. 2007, A&A, 466, 11
Hamuy, M., Phillips, M. M., Suntzeff, N. B., et al. 1996, AJ, 112, 2408
Hamuy, M., Phillips, M. M., Suntzeff, N. B., et al. 2003, Natur, 424, 651
Hicken, M., Challis, P., Jha, S., et al. 2009, ApJ, 700, 331
Hicken, M., Challis, P., Kirshner, R. P., et al. 2012, ApJS, 200, 12
Hillebrandt, W., & Niemeyer, J. C. 2000, ARA&A, 38, 191
Hsiao, E. Y., Conley, A., Howell, D. A., et al. 2007, ApJ, 663, 1187
Jha, S., Garnavich, P. M., Kirshner, R. P., et al. 1999, ApJS, 125, 73
Jha, S., Kirshner, R. P., Challis, P., et al. 2006, AJ, 131, 527
Johansson, J., Amanullah, R., & Goobar, A. 2013, MNRAS, 431, 43
Kamp, I., & Van Zadelhoff, G. J. 2001, A&A, 373, 641
Kasen, D. 2010, ApJ, 708, 1025
Kotak, R., Meikle, W. P. S., Pignata, G., et al. 2005, A&A, 436, 1021
Krisciunas, K., Contreras, C., Burns, C. R., et al. 2017, AJ, 154, 211
Krisciunas, K., Garnavich, P. M., Stanishev, V., et al. 2007, AJ, 133, 58
Li, W., Bloom, J. S., Podsiadlowski, P., et al. 2011a, Natur, 480, 348
Li, W., Leaman, J., Chornock, R., et al. 2011b, MNRAS, 412, 1441
Li, W., Wang, X., Hu, M., et al. 2019, ApJ, 882, 30
Lira, P., Suntzeff, N. B., Phillips, M. M., et al. 1998, AJ, 115, 234
Lü, G., Zhu, C., Wang, Z., & Wang, N. 2009, MNRAS, 396, 1086
Maguire, K., Sullivan, M., Patat, F., et al. 2013, MNRAS, 436, 222
Maoz, D., Mannucci, F., & Nelemans, G. 2014, ARA&A, 52, 107
Matheson, T., Kirshner, R. P., Challis, P., et al. 2008, AJ, 135, 1598
Munari, U., & Zwitter, T. 1997, A&A, 318, 269
Nomoto, K., Iwamoto, K., & Kishimoto, N. 1997, Sci, 276, 1378
Nozawa, T., Wakita, S., Hasegawa, Y., & Kozasa, T. 2015, ApJL, 811, L39
Nugent, P., Kim, A., & Perlmutter, S. 2002, PASP, 114, 803
Olling, R. P., Mushotzky, R., Shaya, E. J., et al. 2015, Natur, 521, 332
Pan, Y. C., Sullivan, M., Maguire, K., et al. 2015, MNRAS, 446, 354
Parrent, J. T., Thomas, R. C., Fesen, R. A., et al. 2011, ApJ, 732, 30
Pastorello, A., Mazzali, P. A., Pignata, G., et al. 2007, MNRAS, 377, 1531
Patat, F., Benetti, S., Cappellaro, E., & Turatto, M. 2006, MNRAS, 369, 1949
Patat, F., Chandra, P., Chevalier, R., et al. 2007, Sci, 317, 924
Patat, F., Chugai, N. N., Podsiadlowski, Ph., et al. 2011, A&A, 530, A63
Phillips, M. M. 1993, ApJL, 413, L105
Phillips, M. M., Lira, P., Suntzeff, N. B., et al. 1999, AJ, 118, 1766
Phillips, M. M., Simon, J. D., Morrell, N., et al. 2013, ApJ, 779, 38
Poznanski, D., Prochaska, J. X., & Bloom, J. S. 2012, MNRAS, 426, 1465
Raski, C., & Kasen, D. 2013, ApJ, 772, 1
Riess, A. G., Macri, L. M., Hoffmann, S. L., et al. 2016, ApJ, 826, 56
Riess, A. G., Kirshner, R. P., Schmidt, B. P., et al. 1999, AJ, 117, 707
Riess, A. G., Li, W., Stetson, P. B., et al. 2005, ApJ, 627, 579
Schaefer, B. E., & Pagnotta, A. 2012, Natur, 481, 164
Schlafly, E. F., & Finkbeiner, D. P. 2011, ApJ, 737, 103
Silverman, J. M., & Filippenko, A. V. 2012, MNRAS, 425, 1917
Silverman, J. M., Nugent, P. E., Gal-Yam, A., et al. 2013, ApJ, 772, 125
Simon, J. D., Gal-Yam, A., Gnat, O., et al. 2009, ApJ, 702, 1157
Soker, N. 2015, MNRAS, 450, 1333
Stanishev, V., Goobar, A., Benetti, S., et al. 2007, A&A, 469, 645
Sternberg, A., Gal-Yam, A., Simon, J. D., et al. 2011, Sci, 333, 856
Stritzinger, M. D., Burns, C. R., Phillips, M. M., et al. 2010, AJ, 140, 2036
```

```
Stritzinger, M. D., Phillips, M. M., Boldt, L. N., et al. 2011, AJ, 142, 156
Taddia, F., Stritzinger, M. D., Phillips, M. M., et al. 2012, A&A, 545, L7
Taubenberger, S., Hachinger, S., Pignata, G., et al. 2008, MNRAS, 385, 75
Tsebrenko, D., & Soker, N. 2015, MNRAS, 447, 2568
Turrato, M., Benetti, S., & Cappellaro, E. 2003, in ESO ASTROPHYSICS
SYMPOSIA 2002, From Twilight to Highlight-The Physics of Supernovae, ed. W. Hillebrandt & B. Leibundgut (Berlin: Springer), 200
Verner, D. A., & Ferland, G. J. 1996, ApJS, 103, 467
Verner, D. A., Ferland, G. J., Korista, K. T., & Yakovlev, D. G. 1996, ApJ, 465, 487
Wang, B., & Han, Z. 2012, NewA, 56, 122
Wang, L. 2005, ApJL, 635, L33
Wang, L., Baade, D., Höflich, P., et al. 2004, ApJL, 604, L53
Wang, L., & Wheeler, J. C. 1996, ApJL, 462, L27
Wang, L., & Wheeler, J. C. 2008, ARA&A, 46, 433
```

```
Wang, X., Filippenko, A. V., Ganeshalingam, M., et al., et al. 2009a, ApJL, 699, L139

Wang, X., Li, W., Filippenko, A. V., et al. 2008a, ApJ, 675, 626

Wang, X., Li, W., Filippenko, A. V., et al. 2008b, ApJ, 677, 1060

Wang, X., Li, W., Filippenko, A. V., et al. 2009b, ApJ, 697, 380

Wang, X., Wang, L., Filippenko, A. V., et al. 2012, ApJ, 749, 126

Wang, X., Wang, L., Filippenko, A. V., Zhang, T., & Zhao, X. 2013, Sci, 340, 170

Wells, L. A., Phillips, M. M., Suntzeff, B., et al. 1994, AJ, 108, 2233

Yang, Y., Wang, L., Baade, D., et al. 2018, ApJ, 854, 55

Yuan, F., Quimby, R., Chamarro, D., et al. 2008, CBET, 1513

Zhang, T., Wang, X., Li, W., et al. 2010, PASP, 122, 1

Zhang, K., Wang, X., Zhang, J., et al. 2016, ApJ, 820, 67

Zhang, K., Wang, X., Zhang, J., et al. 2016, ApJ, 826, 211

Zhao, X., Maeda, K., Wang, X., et al. 2015, ApJS, 220, 20
```